Unveiling the energy alignment across ultrathin 4P-NPD hole extraction interlayers in organic solar cells

Mariam Ahmad[1], Dylan Amelot[2], Hervé Cruguel[2], Bhushan R. Patil[1], Mehrad Ahmadpour[1], Erika Giangrisostomi[3], Ruslan Ovsyannikov[3] Mathieu Silly[4], Lenart Dudy[4], Morten Madsen[1] and Nadine Witkowski[2]*

[1]SDU NanoSYD, Mads Clausen Institute, University of Southern Denmark, Sønderborg DK-6400, Denmark;

[2]Sorbonne Université, UMR CNRS 7588, Institut des Nanosciences de Paris, F-75005 Paris, France

[3]Institute Methods and Instrumentation for Synchrotron Radiation Research, Helmholtz-Zentrum Berlin GmbH, Albert-Einstein-Straße 15, 12489 Berlin, Germany.

[4]Synchrotron SOLEIL, L'orme des merisiers, Saint- Aubin, BP 48, 91192 Gif- surYvette, France

ABSTRACT

Molecular thin films of N,N′-di-1-naphthalenyl-N,N′-diphenyl [1,1′:4′,1″:4″,1‴-quaterphenyl]-4,4‴-diamine (4P-NPD) have been demonstrated to function as efficient exciton blocking layers in organic solar cell devices, leading to improved device performance by minimizing exciton losses and by providing hole extraction selectivity. However, the exact mechanisms have been debated, as ultrathin thicknesses of less than one nm are required to observe optimized device performance improvements. In this work, we conduct photoelectron spectroscopy to gain information about core levels, HOMO/LUMO levels and work functions for the hole extraction side of an organic solar cell device consisting of the small molecule tetraphenyldibenzoperiflanthene (DBP) as an electron donor, 4P-NPD for exciton blocking/hole extraction, the latter being in contact with the hole transport layer,

MoO_x. Using is-situ deposition during characterization, we demonstrate that a negative HOMO energy offset increases with 4P-NPD thickness on the DBP donor layer, which cannot account for the improvement observed in device performance. Investigation of the 4P-NPD/MoO_x interface, on the other hand, reveals shifts of the electronic levels in 4P-NPD and a band alignment that favours hole extraction, while blocking for exciton/electron leakage. This appealing behaviour is enhanced for ultrathin 4P-NPD films of less than one nm. Thus, the exciton blocking/hole extraction behaviour of 4P-NPD interlayers in organic solar cell devices is confirmed and understood from the detailed energy alignment across both interfaces, as extracted from the in-situ photoelectron spectroscopy studies.

INTRODUCTION

Organic solar cells (OSCs) have received a lot of attention over the last two decades due to their mechanical and design flexibility, non-toxic materials, and cost-effective manufacturing routes, which makes them promising candidates for mass production and completely new solar cell integration schemes. The early OSCs struggled with low power conversion efficiencies (PCEs), but OSCs have now reached PCEs above 18% [1], and the possibility of widespread commercialization is therefore just around the corner. However, to make this a reality, and make OSC truly competitive with Si-based solar cells, there is still a need to optimize their device performance further. One of the processes that has a significant effect on the PCE of OSCs is exciton dissociation at the donor/acceptor interfaces. This process is challenged by the short exciton diffusion lengths in organic compounds, around 10-30 nm depending on the specific material system [2,3], which may result in a loss of excitons and thereby also of the photocurrent and PCE. Furthermore, exciton quenching might occur at the interfaces, resulting in a lower PCE [4]. The latter can be overcome by implementing an exciton blocking layer (EBL) between the electron donor and the anode contact [4-6], which is selective to hole extraction. Typical anode contact layers that benefit from such interlayers are high work function

n-type metal oxides, such as molybdenum oxide (MoO_x)[7-8]. The role of such an interlayer is to limit leakage currents and exciton quenching at the anode contact layer, thereby enhancing exciton diffusion and free charge carrier generation in the device. We have recently demonstrated that ultra-thin anode interlayers of N,N′-di-1-naphthalenyl-N,N′-diphenyl [1,1′:4′,1″:4″,1‴-quaterphenyl]-4,4‴-diamine (4P-NPD), which is also known as a blue emitter in OLEDS [9], results in a 24 % higher PCE in DBP/C_{70} solar cells [10]. Surprisingly, the increase was observed only for ultra-thin interlayers of 4P-NPD, of less than one nm, pointing to a major role of the interface in the process. While part of this effect can be understood from a device point-of-view by increased series resistance and optical interference effects for thicker 4P-NPD exciton blocking layers [10], the true role of the interface between the 4P-NPD interlayer and the DBP active layer in this process has not yet been investigated. This study utilises synchrotron-based photoelectron spectroscopies, namely soft X-ray photoemission spectroscopy (PES) and Near-edge X-ray Absorption Fine Structure (NEXAFS), to unveil the electronic energy level alignment between the electron donor tetraphenyldibenzoperiflanthene (DBP) and the anode interlayer 4P-NPD, when in contact with the high work function anode contact layer MoO_x. By this, we reach a clear understanding of the mechanism behind the device improvement that is evidenced for ultrathin 4P-NPD anode interlayers.

a)

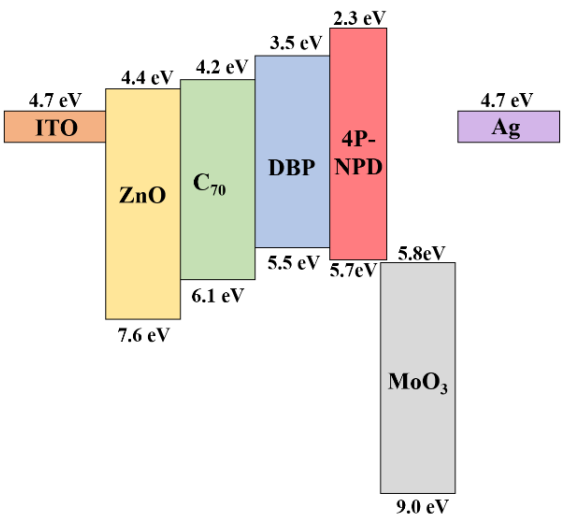

b)

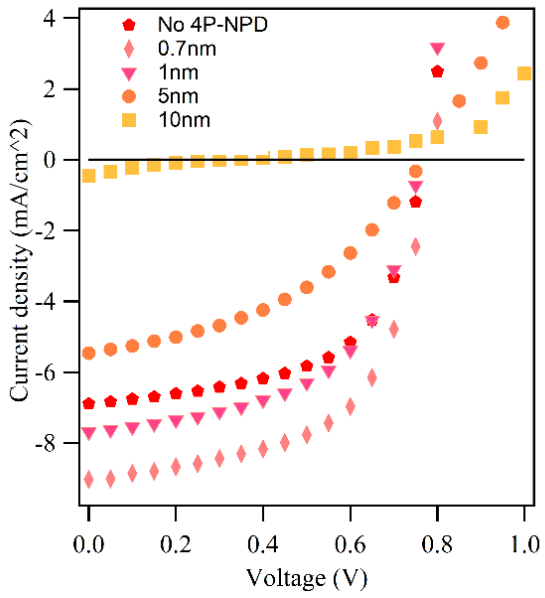

c)

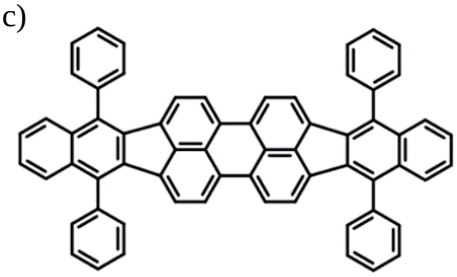

d)

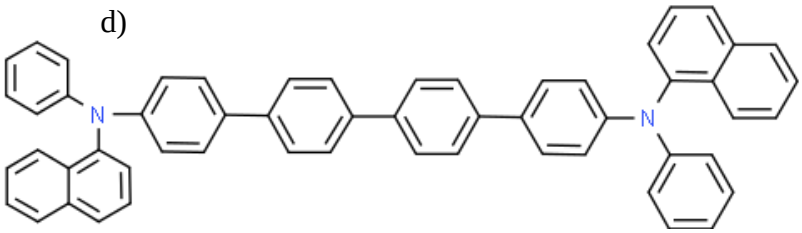

Figure 1. a) Organic solar cell stack and individual layer's energy levels (based on literature values) for devices containing 4P-NPD as an EBL, b) J-V characteristics for OPV devices containing varying thicknesses of 4P-NPD [10]. Molecular structure of c) DBP and d) 4P-NPD studied in this work.

RESULTS AND DISCUSSION

Figure 1a shows the components of the 4P-NPD based solar cell of interest here and their respective energy levels as determined by cyclic voltammetry [10] for individual layers. Figure 1b shows the J-V characteristics for the same solar cells with different thicknesses of 4P-NPD as an EBL [10].

According to the energy level diagram, a thick layer of 4P-NPD would play the role of both exciton blocking and hole extraction, as the energy levels are close-to-optimum aligned, although there is a negative HOMO offset of 0.2 eV between DBP and 4P-NPD in this scenario. The J-V characteristics show that the best performing cells are the ones with an ultrathin film of 4P-NPD (0.7 nm) and that the device performance decreases as the 4P-NPD thickness increases, with the worst performing cells having the thickest 4P-NPD layer (10 nm). The fact that the ultrathin films enhance the device performance suggests that the energy level alignment at the 4P-NPD interface plays a crucial role, which to date has not been investigated and elucidated further.

In-situ depositions of DBP and 4P-NPD followed by photoelectron spectroscopy measurements were conducted to investigate the C1s core levels, HOMO and LUMO states, and work functions for pristine DBP layer, pristine 4P-NPD layer and 0.75 nm of 4P-NPD interlayer deposited on pristine

DBP layers. The C1s spectra are displayed in figure 2a; the absolute binding energies of the main peaks have been determined to be 284.45 eV, 284.46 eV and 284.75 eV for DBP, the interlayer and 4P-NPD, respectively. In addition to the main peak, the C1s spectrum for 4P-NPD presents a feature at higher binding energies, which can be attributed to the carbon atoms participating in a C-N bond, as suggested by its relative binding energy position [11]. The ratio of C-C:C-N evaluated to 6.6+-0.5 underestimates the C-C contribution that could be an indication that α-NPD is also present in the deposited layer. The C1s spectrum recorded for the interlayer has its main peak located at the same binding energy as DBP, and also presents a shoulder at higher binding energies as 4P-NPD. Secondary electron cut-off spectra were recorded to determine the work functions of DBP, the interface and 4P-NPD, which are presented in Fig. 2(b). The work functions are estimated to be 4.34 eV, 4.30 eV and 4.02 eV, for DBP, interlayer and 4P-NPD respectively, with an error bar of 0.05 eV. The pre-edge feature present for pristine DBP may originate from irregularity in the molecular layer [12]. The results show that the work function for the interlayer almost matches the one of DBP and deviates from pristine 4P-NPD.

The valence band region spectra presented in Fig. 2(c) have been used to determine the valence band maxima (VBM), corresponding to the point that intersects the linear fit of the valence band with the baseline. VBM is estimated to be 0.92 eV, 1.15 eV and 1.50 eV below the Fermi level for DBP, the interlayer and 4P-NPD, respectively, with an error bar of 0.05 eV. Note that the valence spectrum for DBP is in good agreement with the one recorded by Kirchhuebel *et al* on a double DBP layer [13]. Furthermore, NEXAFS measurements were conducted to investigate the unoccupied energy levels. Fig. 2(d) shows the NEXAFS C K edge spectra for DBP, the interface and 4P-NPD. The NEXAFS spectra show the transitions from the C1s core levels to the LUMO π* orbitals (below 290 eV) and σ* orbitals (above 290 eV) [14]. The NEXAFS spectrum for DBP presents a main feature at 285.3 eV and is very similar to the spectrum recorded on pristine DBP [15]. The NEXAFS spectra for 4P-

NPD and the interlayer have their main feature at 285.2 eV contrary to what was observed for core level and valence band. In the NEXAFS technique, the presence of core holes in the process prevents one from determining the absolute energy position of empty states, as it can be obtained from e.g., inverse photoemission or scanning tunnelling spectroscopies [16]. Moreover, the determination of molecular orbital contributions would require ab-initio calculations that go beyond present research's scope. We have thus determined the relative positions of conduction band minimum (CBM), which is of crucial interest for device performance, for pristine DBP, 4P-NPD and interlayer by determining the signal on-set, as for the valence band. The CBM is found it to be nearly identical for pristine DBP and the interlayer, whereas it is found to be 0.4 eV higher for pristine 4P-NPD.

To better understand the nature of the 4P-NPD/DBP interface, and to identify any chemical bonding between the two molecules, linear combinations of spectra for DBP and 4P-NPD have been constructed to reproduce the spectra measured for the 4P-NPD interlayer. For this purpose, the C1s spectra in Fig.2(a) have been normalized to the number of carbon atoms present in the molecule, i.e., to N_{DBP}=64 for DBP, to N_{4PNPD}=56 for 4P-NPD, and to $N_{interlayer}$=58.7 for the interlayer, using the simplified formula for semi-infinite homogenous films [17]:

$$N_{interlayer} = N_{DBP}\left(e^{\left(-\frac{d}{\lambda}\right)}\right) + N_{4PNPD}(1 - e^{\left(-\frac{d}{\lambda}\right)})$$

d=0.75 nm being the thickness of the 4P-NPD interlayer, and λ=0.69 nm the attenuation length in graphite at a kinetic energy of 95 eV [18], since the two molecules are essentially composed of carbon atoms. The best adjustment of the interface C1s spectrum (green open circle in Fig.2 (a)) is achieved by shifting the 4P-NPD spectrum by 0.3 eV to lower binding energy with respect to the original position, and by adding the DBP and 4P-NPD spectra in the ratio 0.25:0.75. The adjusted spectrum is presented as a solid green line in Fig.2 (a), and reproduces the interface spectrum reasonably well.

In particular, no additional peaks are required to fit the interface spectrum. However, a binding energy shift of the spectrum for bulk 4P-NPD is necessary, which could indicate charge transfer and related band bending at the interface. A similar procedure has been used to reproduce the interface spectrum in the valence band region, Fig.2 (c), corresponding to the filled electronic levels. Because valence electrons are delocalized, spectra are only normalized to the incoming photon flux. For the valence band region, a DBP to 4P-NPD ratio of 0.3:0.7 is obtained. A good fit is achieved by shifting the 4P-NPD valence spectrum by 0.28 eV towards the Fermi position, confirming for the valence band the same energy shift observed for the core level, and the absence of any new feature that could be a signature of chemical bonding at the interface. From the intensity ratio DBP to 4P-NPD, extracted from both core level and valence band, it is established that the interlayer deposition of 4P-NPD includes a substantial contribution to the interface between DBP and 4P-NPD.

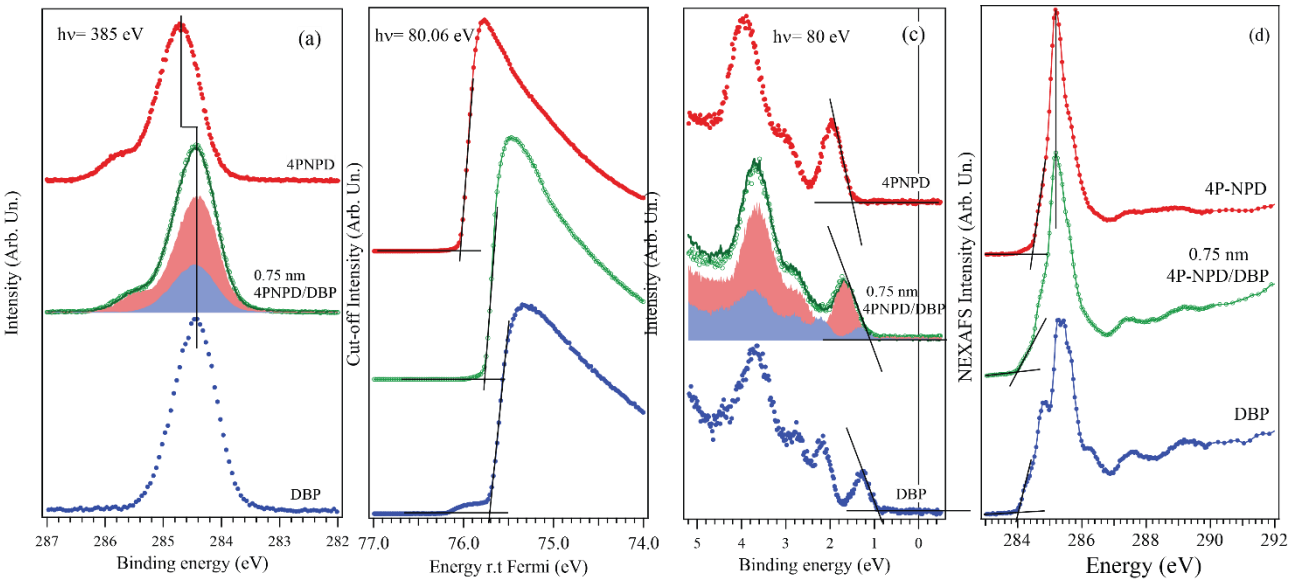

Figure 2. a) C1s XPS spectra, b) Secondary electron cut-off spectra, c) valence band spectra and d) NEXAFS C K edge spectra for of DBP (blue), the interface (green) and 4P-NPD (red). In a) and c) a linear combination consisting of shifted, weighed and added DBP and 4P-NPD spectra is included

(dark green solid line) together with respected contributions from DBP and 4P-NPD. A Shirley background has been subtracted from the core level and VB spectra using CasaXPS.

The results above characterize the interlayer of 0.75 nm, consisting of a weakly interacting mixture of DBP and 4P-NPD without evidence of chemical bonding or hybridization. By measuring the work functions, the absolute energies of VBM and the relative energies of CBM extracted from NEXAFS, we can draw the full energy line-up at the interface, as depicted in Fig. 3 and summarized in Table 1. The reference for LUMO position has been determined by adding the transport gap of 3.3 eV to the VBM of DBP, measured on a thick layer of DBP by Kirchhuebel et al. [13].

Table 1. Values of energy levels relative to Fermi position. * values deduced from NEXAFS shows relative energy with respect to bulk DBP LUMO on-set, calculated from HOMO on-set of DBP using a transport gap of 3.3 eV taken from [13].

	HOMO	LUMO	Work function	Transport gap*
DBP bulk	-0.92 eV	2.38 eV [5]	4.34 eV	3.3 eV *
~0.75 nm 4P-NPD/DBP	-1.15 eV	2.28 eV *	4.30 eV	3.43 eV *
4P-NPD bulk	-1.50 eV	2.78 eV*	4.02 eV	4.28 eV *

We note that the energy alignment extracted from such soft X-ray spectroscopies across interfaces is typically very different from those extracted from cyclic voltammetry measurements of the individual layers, like in Fig.1a, which do not include interfacial electronic interplay. Therefore, in general one should be careful with concluding on band alignment and energetic offsets across interfaces from any measurement of the individual layers alone especially in the case of ultra-thin layers. Fig.3 shows the energy alignment across the DBP and 4P-NPD interface extracted from Fig.2b, 2c and 2d, revealing

a negative HOMO offset of ~ 0.2eV from bulk DBP to the interface region, which increases to ~0.6 eV when moving into bulk 4P-NPD. This could be the signature of charge transfer across and accumulation at the interface, inducing an interface dipole which however is not confirmed by the vacuum level that remains almost aligned at the interface [19]. If charge transfer occurs, it is extremely limited and cannot fully explain the large energy shift observed in the valence region of the interlayer. Moreover, the appearance of interfacial states in the semiconducting gap, which could pin the Fermi position, is not observed in the interlayer region. As for several other organic-organic heterojunctions, Van der Waals interactions dominate the 4P-NPD/DBP interface, therefore it can be considered as a non-interacting system [20]. Thus, the observed energy alignment at the interface must originate from a different process. Indeed, it has been evidenced on organic systems [13, 21] that the transport gap is reduced when decreasing the thickness of organic films due to the reduction of polarizability, related to the local chemical environment occurring for very thin layers. The rugosity at the interface and molecular packing may also affect the transport gap through the change of polarizability screening. The transport gap from a thick 4P-NPD layer to the 0.75 nm layer is reduced by ~0.85 eV in the present system, which is of the same order of magnitude as what is already measured for other organic systems [13]. Such a change of polarizability can account for the energy shift observed on the valence and core levels at the interface.

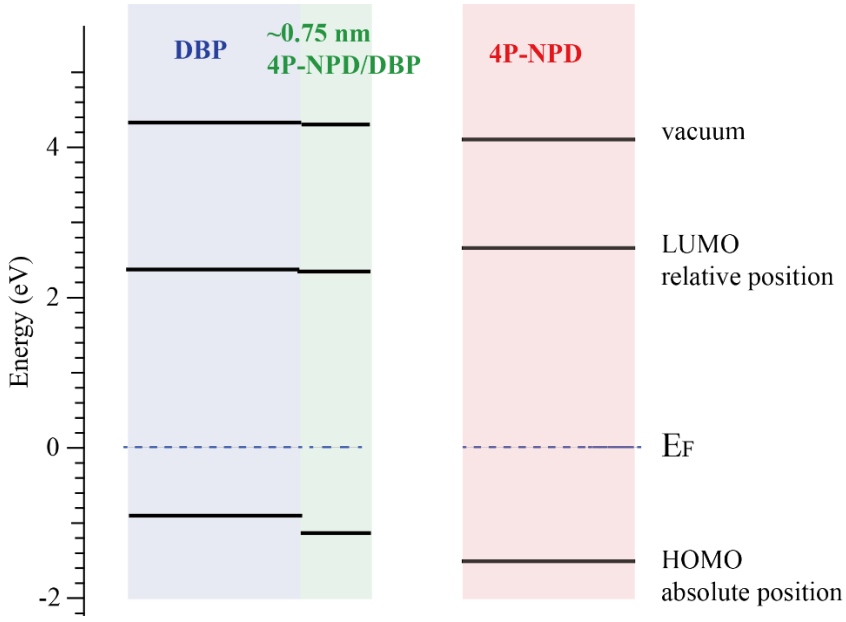

Figure 3. Absolute HOMO energy level alignment at the DBP/4P-NPD interface and relative LUMO on-set using a transport gap of 3.3 eV for DBP [13]. Data are extracted from Fig. 2b-c-d.

Still, the detailed role of the interface in providing exciton blocking and hole extraction properties for ultrathin 4P-NPD EBL thin films remains unanswered. For thick layers of 4P-NPD, the measured negative HOMO offset of about 0.6 eV represents a hole extraction barrier in solar cells. The presence of such barrier can explain the negligible current density measured for a 10 nm layer of 4P-NPD in the solar cell stack depicted in the Fig. 1b. At the interface, this is very different as the offset is reasonably small, possibly facilitating hole extraction across the interface, although not displaying the optimum positive HOMO offset. The LUMO position at the interface nearly aligns with the one from DBP, and thus opens for electron leakage, impeding any hole extraction selectivity of the 4P-NPD interlayer. An investigation of the counter interface with molybdenum oxide is required to fully understand the behaviour of the ultra-thin 4P-NPD as anode interlayer. A similar 4P-NPD deposition of about 0.75 nm has thus been measured on a thermally evaporated MoOx substrate. The valence band and photoemission onsets allow for the description of the full band alignment, as displayed in Fig.4. Absolute HOMO positions for MoOx and 4P-NPD interlayer are estimated to 2.8 eV and 0.5

eV respectively. Vacuum levels have been extracted from the present work and are estimated to 5.1 eV and 4.6 eV for MoOx and 4P-NPD interlayer respectively. The LUMO position of DBP is obtained as in Fig.3, whereas the LUMO position for the and 4P-NPD interlayer is estimated by adding the gap from table 1 to the valence band maximum. The conduction band of MoO_x is estimated by adding a gap of 3 eV to the valence band maximum [22]. The energy diagram at the interface of 4P-NPD with MoO_x resembles the one already measured on the very similar α-NPD/MoO_3 system [23], with a lower interface dipole in our system due to the moderate work function of 5.1 eV of the MoO_x sample. Such a dipole is characteristic of electron transfer from the organic layer to the MoO_x layer. A band bending is commonly evidenced in organic layers close to the MoOx interface due to a pinning of the HOMO edge at the Fermi level, resulting from electron transfer, providing a downwards shifted HOMO level for increasing thickness of the organic layer [7]. As observed for the present system, and as evidenced extensively for MoO_x/organic interfaces [7], hole extraction proceeds via electron transfer from the conduction band of MoO_x to the HOMO level of the organic layer, which is energetically favourable for the energy band line-up observed. Such mechanism is enhanced for higher work function MoO_x, which presents larger band bending at the interface. Furthermore, and importantly, for thicker 4P-NPD layers, the HOMO level is expected to relax to its bulk position for about 10 nm, as already seen on other organic systems [24], becoming less favourable for the holes to be extracted from DBP layer. This can explain the better performance of the devices for very thin 4P-NPD layers. Considering the exciton/electron leakage from DBP to MoO_x, such leakage is precluded with the insertion of the 4P-NPD layer due to the expected higher-lying LUMO level of 4P-NPD, caused partially by the shifted electronic levels at the MoO_x surface. Such shift is pronounced for very thin 4P-NPD layers, thus preserving the exciton blocking properties of 4P-NPD and improving hole extraction selectivity at the interface for ultra-thin layers.

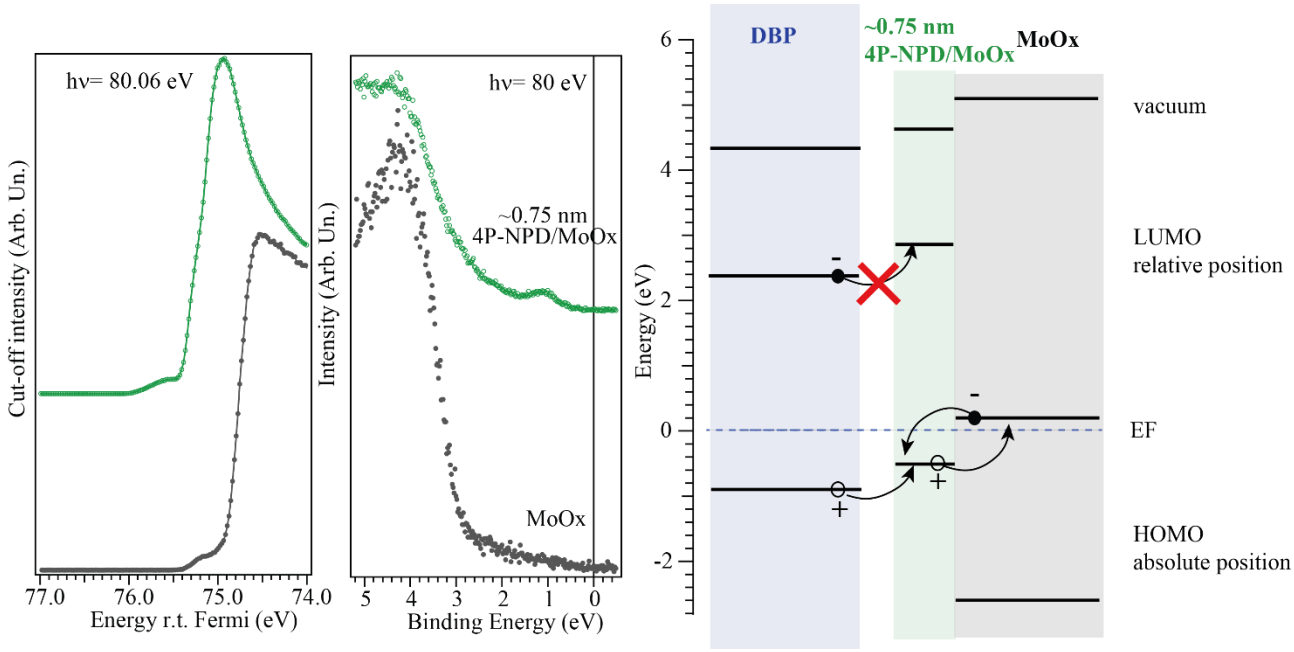

Figure 4. Left : Secondary electron cut-off spectra and valence band spectra for MoOx and 0.75 nm 4P-NPD/MoOx; right : energy level alignment at DBP and 4P-NPD/MoOx interlayer.

We note that the interlayer in the present photoelectron spectroscopy studies is estimated to be 0.75nm thick, which in fact is very close to the ideal thickness observed in the devices for the 4P-NPD layer. The energetic line-up at the interface, which is affected by dipole effects, can explain the positive influence of the interface in the exciton blocking and hole selective extraction properties of 4P-NPD in organic solar cells, as also demonstrated experimentally in devices. It highlights the importance of interfacial electronic interplay in the performance of organic solar cells.

CONCLUSIONS

In this study, we have explored the electronic state interplay of 4P-NPD/DBP interlayer to shed light on the mechanisms behind the role of ultrathin 4P-NPD layers as efficient exciton blocking and hole extracting layers in organic solar cells. In-situ XPS and NEXAFS measurements have been conducted to study the core levels, HOMO and LUMO levels and work functions of the electron donor DBP, the anode interlayer 4P-NPD and the 4P-NPD/DBP interface, as they appear in organic solar cell

devices, to draw a comprehensive energy band alignment diagram. Weak interaction at the interface is accompanied by a negative HOMO offset that increases with 4P-NPD thickness. This picture is complemented with investigating molybdenum oxide anode contact layer in contact with the ultra-thin 4P-NPD anode interlayer, revealing a strong upward shift of all electronic levels in 4P-NPD, providing a barrier for electron extraction from DBP and a positive HOMO offset from DBP to 4P-NPD. This favours hole extraction selectivity in the 4P-NPD layer but is also expected to relax for thicker layers, which explains why ultrathin 4P-NPD anode interlayers are ideal for hole extraction selectivity in these devices. These in-situ photoelectron spectroscopy studies therefore fully explain the reason why a thickness of about 0.7nm is optimal for as exciton blocking and charge selective hole extraction in organic solar cells, and why the device performance drops for thicker layers. We note that in-situ vacuum deposition followed by photoelectron spectroscopy, as conducted here, is a powerful experimental technique for obtaining the true energy level alignment and offsets in organic-organic interfaces, which is very relevant for understanding their role in thin film devices, such as organic solar cells.

EXPERIMENTAL SECTION

DBP powder was purchased from Sigma Aldrich and 4P-NPD powder was purchased from Luminescence Technology Corp. MoO_3 powder (99.99 %) was purchased from Sigma-Aldrich. The MoO_x films were prepared at the University of Southern Denmark by thermal evaporation of MoO_3 powder on Si substrates in ultra-high vacuum (10^{-8} mbar) [8].

Electron spectroscopy measurements have been carried out on large scale facilities at BESSY II synchrotron on the PM4 beamline [25] and at SOLEIL synchrotron on TEMPO beamline [26]. NEXAFS and work function measurements were solely conducted at SOLEIL, whereas core levels and valence band have been measured on both places and were found identical except for the

statistics. Thus, the presented core levels data have been measured at the TEMPO beamline whereas valence bands have been measured at PM4 beamline. DBP and 4P-NPD thin films were evaporated in-situ on cleaned n-doped Si wafers at the respective beamlines and measured subsequently without breaking vacuum. At PM4, DBP and 4P-NPD layer of 2 nm and 2.5 nm respectively has been evaporated on silicon for pristine molecular film characterization. 4P-NPD overlayer of 0.75 nm has been evaporated on the DBP pristine film. At TEMPO, 4 nm thick DBP pristine film has been evaporated on silicon, followed with 0.75 nm 4P-NPD, followed with a thick layer of presenting identical spectra like the one obtained at PM4. All spectra were taken in normal emission of the photoelectrons with photon energies of 80 eV for the valence band and work function and of 650 eV for core levels. The overall energy resolution E/ΔE was better than 6000. The binding energy (BE) scale has been calibrated using metallic Ta clamps attached to the sample surface. A Shirley background has been removed from XPS spectra on C1s. Cut-off of secondary electrons has been measured applying -18 eV on the sample. Absorption spectra at carbon K-edge were recorded in a partial electron yield mode in an energy window of 12 eV around the C KLL transition at 250 eV using the same spectrometer as for photoemission in normal emission. The photon energy calibration was achieved by measuring the Au 4f photoelectrons from a gold foil mounted on the manipulator excited by 1st and 2nd order light. The NEXAFS spectra have been normalized using spectra for a clean carbon-free gold surface measured under the same conditions as the samples and normalized to unity at the photon energy of 320 eV following the procedure described in ref. [14]. The overall resolution of the NEXAFS spectra was about 100 meV.

The thickness of the overlayer of 4P-NPD on DBP has been evaluated to 0.75 +/- 0.15 nm from the N 1s signal recorded with kinetic energy centered at 105 eV and using an attenuation of 0.7 nm, as calculated for graphite with the Tanuma Powell and Penn algorithm (TPP2M) [27] since the 4P-NPD molecule is dominated by carbon atoms arranged in benzene rings [28]. The thin-film integration into

organic solar cell devices has been performed using a fabrication protocol like the one demonstrated in ref [10].

AUTHOR INFORMATION

Corresponding Authors:

*N.W: nadine.witkowski@sorbonne-universite.fr

ACKNOWLEDGEMENTS

We thank the beamline specialists and staff at PM4, BESSY and TEMPO, SOLEIL for their help during our beamtimes at the respective synchrotron facilities. The research leading to this result has been supported by the project CALIPSOplus under the Grant Agreement 730872 from the EU Framework Programme for Research and Innovation HORIZON 2020. We also thank the Danish Agency for Science, Technology, and Innovation for providing travel funding through the instrument center DanScatt, and the support from the project 'SMART - Structure of MAterials in Real Time', funded by the Danish Ministry of Higher Education and Science

REFERENCES

[1] Liu, Q., et al. (2020). "18% Efficiency organic solar cells." Science Bulletin **65**: 272.

[2] Firdaus, Y., et al. (2020). "Long-range exciton diffusion in molecular non-fullerene acceptors." Nature Communications **11**(1): 5220.

[3] Sajjad, M. T., et al. (2020). "Long-range exciton diffusion in non-fullerene acceptors and coarse bulk heterojunctions enable highly efficient organic photovoltaics." Journal of Materials Chemistry A **8**(31): 15687-15694.

[4] Hirade, M. and C. Adachi (2011). "Small molecular organic photovoltaic cells with exciton blocking layer at anode interface for improved device performance." Applied Physics Letters **99**(15): 153302.

[5] Grob, S., et al. (2014). "Amorphous vs crystalline exciton blocking layers at the anode interface in planar and planar-mixed heterojunction organic solar cells." Applied Physics Letters **104**(21): 213304.

[6] Caliò, L., et al. (2018). "Benzothiadiazole–triphenylamine as an efficient exciton blocking layer in small molecule based organic solar cells." Sustainable Energy & Fuels **2**(10): 2296-2302.

[7] Meyer, J., et al. (2012). "Transition Metal Oxides for Organic Electronics: Energetics, Device Physics and Applications." Advanced Materials **24**(40): 5408-5427.

[8] Ahmadpour, M., et al. (2019). "Crystalline Molybdenum Oxide Layers as Efficient and Stable Hole Contacts in Organic Photovoltaic Devices." ACS Applied Energy Materials **2**(1): 420-427.

[9] Sun, N., et al. (2014). "A white organic light-emitting diode with ultra-high color rendering index, high efficiency, and extremely low efficiency roll-off." Applied Physics Letters **105**(1): 013303.

[10] Patil, B. R., et al. (2017). "4P-NPD ultra-thin films as efficient exciton blocking layers in DBP/C70 based organic solar cells." Journal of Physics D: Applied Physics **50**(38): 385101.

[11] Ligorio, G., et al. (2015). "Organic Semiconductor/Gold Interface Interactions: From Physisorption on Planar Surfaces to Chemical Reactions with Metal Nanoparticles." ChemPhysChem **16**(12): 2602-2608.

[12] Helander, M. G., et al. (2010). "Pitfalls in measuring work function using photoelectron spectroscopy." Applied Surface Science **256**(8): 2602-2605.

[13] Kirchhuebel, T., et al. (2020). "Role of Initial and Final States in Molecular Spectroscopies: Example of Tetraphenyldibenzoperiflanthene (DBP) on Graphite." The Journal of Physical Chemistry C **124**(36): 19622-19638.

[14] Stöhr, J. and R. Gomer (1992). NEXAFS Spectroscopy, Springer.

[15] Grob, S., et al. (2015). "Solvent vapor annealing on perylene-based organic solar cells." Journal of Materials Chemistry A **3**(30): 15700-15709.

[16] Gao, Y. (2010). "Surface analytical studies of interfaces in organic semiconductor devices." Materials Science and Engineering: R: Reports **68**(3): 39-87.

[17] Fadley, C.S. (1997) Electron Spectroscopy: Theory, Techniques and Applications, Volume 2 (Ed C. R. Brundle, Arthur D. Baker), Academic Press.

[18] Tanuma, S., et al. (2011). "Calculations of electron inelastic mean free paths. IX. Data for 41 elemental solids over the 50 eV to 30 keV range." Surface and Interface Analysis **43**(3): 689-713.

[19] Hill, I. G., et al. (2000). "Organic semiconductor interfaces: electronic structure and transport properties." Applied Surface Science **166**(1): 354-362.

[20] Hill, I. G. and A. Kahn (1998). "Energy level alignment at interfaces of organic semiconductor heterostructures." Journal of Applied Physics **84**(10): 5583-5586.

[21] Hill, I. G., et al. (2000). "Initial stages of metal/organic semiconductor interface formation." Journal of Applied Physics **88**(2): 889-895.

[22] Kröger, M., et al. (2009). "P-type doping of organic wide band gap materials by transition metal oxides: A case-study on Molybdenum trioxide." Organic Electronics **10**(5): 932-938.

[23] Kröger, M., et al. (2009). "Role of the deep-lying electronic states of MoO3 in the enhancement of hole-injection in organic thin films." Applied Physics Letters **95**(12): 123301.

[24] Irfan, et al. (2011). "Strong interface p-doping and band bending in C60 on MoOx." Organic Electronics **12**(9): 1588-1593.

[25] Giangrisostomi, E., et al. (2018). "Low Dose Photoelectron Spectroscopy at BESSY II: Electronic structure of matter in its native state." Journal of Electron Spectroscopy and Related Phenomena **224**: 68-78.

[26] Polack, F., et al. (2010). "TEMPO: a New Insertion Device Beamline at SOLEIL for Time Resolved Photoelectron Spectroscopy Experiments on Solids and Interfaces." AIP Conference Proceedings **1234**(1): 185-188.

[27] Tanuma, S., et al. (2003). "Calculation of electron inelastic mean free paths (IMFPs) VII. Reliability of the TPP-2M IMFP predictive equation." Surface and Interface Analysis **35**(3): 268-275.

[28] Hüfner, S. (2003). Photoelectron spectroscopy: principles and applications (Springer-Verlag Berlin Heidelberg).